Seismic Analysis and Design of Flared Bridge Columns

by

Hisham Nada[1], David Sanders[2], and M. Saiid Saiidi[3]

ABSTRACT

Past earthquakes have shown that flared columns are susceptible to premature shear failures. In the 1994 Northridge Earthquake, shear failures were caused by a plastic hinge forming at the base of the flare and a subsequent increase in the level of column shear demand above design levels. This paper presents an experimental and analytical study that is examining new details for flared columns and joints. The primary feature is a gap at the top of the column and the amount of transverse flare reinforcement. Two two-column bents were tested on the shake table to examine dynamic effects as well as column and beam interaction. The test specimens had different amounts of confining reinforcement in the flare. The details had an overall displacement ductility that was well above 6. Test also showed that gap started to close at a displacement ductility level below 6.

KEYWORDS: bent; bridge; flared columns; seismic; shake-table

1.0 INTRODUCTION

Design of flared columns to resist earthquake loading is a complicated issue due to the changing cross section along the column length. Past earthquakes have shown that flared columns could have poor behavior due to the large increase of column flexural capacity at the top of the column. The increased capacity can cause the plastic hinge region to shift away from the column-beam interface into the column. This causes the column to behave like a much shorter column and therefore have increased shear demand. The shifting of the hinge and the larger shear demand was not included in many previous designs and has led to brittle shear column failures. Brittle shear behavior may lead to significant damage and/or complete collapse of the bridge.

It was believed that if the flares had low longitudinal and transverse reinforcement ratios, they would spall during earthquakes. Therefore, the column core would be the element remaining to resist the earthquake. Experiments and past experience proved that even lightly reinforced flares contribute to increasing the column's flexural capacity (Sanchez et al 1997). To solve this problem, the California Department of Transportation (Caltrans) has developed new details attempting to separate the flared portion of the column from the overall flexural stiffness and capacity of the column. This is achieved by separating the flare from the bent cap using a gap between the top of the flare and the beam bottom surface, see Fig. 1. Caltrans' recommendations came as a result of single column slow-cyclic tests (Sanchez et al 1997) and not on system bent tests. The purpose in conducting shake-table bent tests is to study the effectiveness of the flare detail and to examine the behavior within the joint region as well as the overall system response. Four bents will be tested as part of the overall study. Two bents will be flexurally dominated while two will have shorter column heights to cause higher column shear demand. The columns are pinned at the base with a two-way hinge. Within each bent of similar height, the amount of flare transverse

[1] Principal Engineer, Alrabiah-Cowi Consulting Engineers, Dammam, KSA
[2] Associate Professor, Dept. of Civil Engineering, University of Nevada, Reno, Nevada, 89557
[3] Professor, Dept. of Civil Engineering, University of Nevada, Reno, Nevada, 89557

reinforcement will be varied. In one case the amount of transverse reinforcement in the flare will be in accordance with current Caltrans' guidelines while in the second case, the amount of reinforcement will be reduced in accordance to a proposed Caltrans detail. This document will focus on the tall bents tested (LFCD1 & LFCD2), which are flexurally dominated. The experiments were conducted at the Large-Scale Structures Laboratory at the University of Nevada, Reno.

2.0 MODEL DESIGN

2.1 Column Design

A survey was made of existing bridges in California to develop a prototype. Because the model will be used for new bridge detailing, only bridges that were designed according to the latest code provisions were considered in the survey. Based on these details and the 445 kN vertical load capacity of a single shake table, a 1/5-scale model was developed. The vertical axial load acting on each column was based on 10% of $f'_c A_g$ where A_g is the gross column cross section and f'_c is the concrete compressive strength

The 10% level was set as a typical upper range for the majority of new columns in regular bridges. This level resulted in a total axial load of 451.5 KN. In order to distribute this load along the length of the bent, lead buckets in combination with small rams were used. The other key details for the columns are given in Table 1 and shown in Fig. 2. All reinforcement is Grade 60 (414 MPa) to conform to current design. Some dimensions that cannot be scaled due to practical issues, like concrete cover, are kept within the minimum range that allows for practical use. The flexurally-dominated tall columns had a clear height of 1,625.6 mm while the shorter columns had a height of 939.8 mm. The bents described in this paper had the taller columns.

2.2 Flare Design

Flare reinforcement layout was calculated by scaling the prototype dimensions. Current Caltrans recommendations state the following (Caltrans Seismic Design Criteria):

- The gap width is calculated based on the estimated rotation at the top of column so as to prevent gap closure. The minimum height of the gap is 50 mm.
- The longitudinal flare reinforcement is nominal. Spacing between longitudinal flare reinforcement shall not exceed 450 mm and not less than 150 mm.
- The transverse flare reinforcement ratio (ρ_h) in the upper 1/3 of the flare height is equal to 0.45%±0.05 while that ratio for the lower 2/3 of the flare height is equal to 0.075%±0.025.

Where;

$\rho_h = 2 A_b / S D$
S = Spiral pitch
D = Column diameter
A_b = Area of spirals

To investigate these provisions and their effectiveness, two flare details were developed. The first one had a flare lateral reinforcement ratio that complied with the above-motioned provisions. The second detail had constant lateral flare reinforcement ratio along the total height of the flare. This was set to the lowest value of ρ_h=0.075%.

2.3 Bent Cap Design

To match the prototype, the center-to-center span of the bent should have been 2,286 mm. Since it was decided to use lead to apply the axial load, there was insufficient spacing between the columns to accommodate all of the lead. For this reason, the span was increased to 2,718 mm. The beam's depth was also increased in order to have the same relative flexural stiffness between the columns and the beam as

in the prototype. The bent cap was designed according to Caltrans' recommendations, which states that the beam capacity should be 1.2 times the capacity of the plastic hinge in the column. This is done to assure that a plastic hinge would form in the columns rather than the beam.

3.0 TESTING

3.1 Test Setup

The specimens were constructed at the University of Nevada, Reno. A total of 110 strain gauges were attached to reinforcement in the columns, flares and the beam-column connections. Material properties for the specimens are summarized in Tables 2 and 3.

The footing was tied to the shake table using prestressed steel bars to prevent any uplift during the test. The axial load was applied using steel buckets filled with lead blocks. The maximum vertical load capacity the shake table can sustain limited the weight of the specimen plus lead to 445 KN. The specimen weight was about 133.4 KN including the footing. The total axial load for both columns was 451.4 KN. In order to reduce the weight on the table, 178 KN of axial load was modeled using self-equilibrating rams in combination with the mass rig, see Fig. 3. The mass rig is a steel structure supported by frictionless pins so that it allows the system to move laterally without restraining it. The four rams were mounted over the two column and the mass rig was connected to the specimen with a rigid link and a load cell.

Beside the strain gauges, 34 transducers were used to measure the curvature along the column height and along the beam, beam-column connection in-plane displacements, out-of-plane displacements and horizontal movement of the bent and the column base. Accelerometers were mounted on the table, on top of the specimen and the lead, on the mass rig and in the transverse direction.

3.2 Runs and Observations

The loading procedure for the specimen consisted of a series of earthquake runs. This loading sequence was chosen so that it would capture the important points like cracking, yield and ultimate. The specimens were excited with scaled versions of the Sylmar record (Northridge Earthquake, 1994). The acceleration of the original record was multiplied by a factor. The following numbers are the factors used for the series of earthquake records: 0.15, 0.5, 0.75, 1.0, 1.25, 1.5, 1.75, 2.0, 2.125, 1.75, and 1.75 times Sylmar. During the test of LFCD1, it was observed that after 2.125 Sylmar the frequency of the specimen dropped dramatically from an initial value of 3.2 Hz. to 1.0 Hz. Because of this large drop it was decided not to increase the motion but to repeat lower motions to characterize the system. The 1.75 Sylmar record was repeated twice for LFCD1 and once for LFCD2. Fig. 4 shows final crack patterns for LFCD1 while Fig. 5 shows final crack patterns for LFCD2. Observations during the test and maximum strain level reached are summarized in Tables 4 and 5.

The relative rotation between the beam and the column increased dramatically after yielding of the reinforcement in the gap region causing the gap to be closed for both specimens. The curvature trend along the flare height proportionally increased with elevation for LFCD2 while this is not the case for LFCD1, see Figs. 6 and 7. LFCD1 had increased curvature at the base of the flare caused by increased confinement in the flare. The accumulative load-deflection curves of the two specimens for all runs are shown in Fig. 8.

Fig. 9 shows the envelope curve for the two specimens. The graph shows a kink in the load-deflection envelope at approximately 70 mm for LFCD1 and LFCD2 followed by a large increase in the overall stiffness. This behavior was due to the gap closure that caused an increase in the load carrying capacity that was predicted to be 160.1 KN. The difference of gap closure effect on the load-displacement envelope of the two specimens was because of concrete crushing of LFCD2 at the top portion of the flare. This behavior reduced the capability of the flare to transfer force to the beam.

The experiments were stopped due to concerns about the overall stability of the specimen. Since the reinforcement at the top of the columns was near the strain-hardening region, bar fracture could cause the top of the column to quickly lose moment capacity. It was also observed that while the last two runs had smaller input accelerations, the displacement histories were the same as 2.125 Sylmar. Increased moment capacity did lead to shear cracking in the middle portion of the flare and a shear crack in the beam as well as concrete crushing in the middle of the flare (see Figs. 4c and 5c).

LFCD2 shows wider and longer shear crack plus many small shear and flexural cracks spread over the beam span. Another important observation is that the shear crack appearing in LFCD1 started after a distance of about d/2 from the end of the flare. In LFCD2, this distance of d/2 is measured from the column core. This shows that the extensive concrete spalling shifted the primary load path to the core of the column in LFCD2.

4.0 POST-TEST ANALYSIS

4.1 Finite Element Analysis

After extracting the results from the data obtained from the tests, a finite element analysis was done using a program called DIANA. The test specimens were modeled as 2-D plane stress elements with the reinforcement modeled as 2D truss elements (see Fig. 10). Drucker-Prager failure envelope was used for concrete accompanied with a tension cut-off to model the brittle tensile strength of the concrete. The strain-rate effect was taken into consideration by increasing the concrete compressive strength and the yield stress of the steel reinforcement. For the concrete, the test cylinder strength was multiplied by 0.85 to convert from the uniaxial test strength to the specimen strength and then by 1.2 to account for the strain rate effect. This resulted in a net factor of 1.02. The reinforcement yield strength was multiplied by 1.2 to account for strain rate effects. The ultimate stress properties were not modified.

Contact elements were used in the form of non-linear springs at the location of gap closure. These elements stiffness was specified to be zero until gap closure occurred where their stiffness jumped to transfer the loads through the regions in contact. The frames were loaded vertically with distributed loads equivalent to the lead weight. The lateral load was specified as a single load from one side of the beam. The loading was performed in one direction until the failure of the system. The analysis was repeated by applying the lateral load in the opposite direction of the system to compare the analysis with the complete load-displacement curve envelopes from the experiments.

The results are shown in the Figs. 11 and 12. The curves show very good correlation with the tested specimens. Table 6 summarizes the obtained results compared to the experimental ones. This analysis was used as the base for analytical parametric study that will be published in subsequent papers.

4.2 Strut-and-Tie Model

The above FE analysis was used to construct a Strut-and-Tie Model (STM) for the disturbed-regions (D-regions) that existed in the system. The need for the STM was raised as a result of the fact that simple analysis based on section analysis did not succeed in estimating the maximum capacity of the system. Also, the STM helps to understand the stress flow and can be used as a powerful design tool. The system's D-regions are shown in Fig. 13 based on Saint Venant's principle: the base hinge region, the flare region and the beam-column connection region. With the principal stress trajectories and the cracking patterns were obtained from the FE analysis and the experimental results, a STM for each portion of the structure was constructed. A detailed description about the STM will be published in subsequent papers.

The above analysis led to the construction of the models shown in Fig. 14 for the columns. The experimental data showed the yielding of the columns longitudinal reinforcement, the

premature yielding of the base hinge dowels and the yielding of the flare hoops as well. The yielding of the flare hoops was caused by a spreading of the forces into the flare. Limiting this reinforcement would limit the spreading of forces into the flare. The results were used in calculating the system capacity by evaluating the forces in the ties that represent the base hinge dowels, the flare hoops and the column longitudinal bars at the gap region. Having the lateral force as the unknown, the system is statically determinate. The above procedure resulted in the values shown in Table 7. The model was able to predict the maximum capacity efficiently.

5.0 CONCLUSIONS

- Both of the Caltrans details are well above the target displacement ductility limit of 6 that is recommended by Caltrans.
- While the ductility level is adequate, the closure of the gap increased the capacity at the top of the column that led to shear cracks in the columns. This behavior is undesirable for it might lead to brittle shear failure the columns.
- The gap closure affected the plastic hinge formation at the top of the column, and hence, transferred higher loads to the bent cap that resulted in shear cracks in the bent cap.
- An analysis or design based on only the column core stiffness did not accurately model the observed behavior. Analysis that is more representative using Strut-and-Tie model of the system was able to predict the capacity of the system. It was also able to model the behavior in the joint region.
- While the flare gap closure did cause damage in the beam, it also provided for increase strength at a point in the load-displacement history where the load was beginning to decrease. If the beam and column were designed for gap closure, gap closure could be used as a way to increase overall displacement capacity.

6.0 ACKNOWLEDGEMENTS

The authors would like to express their appreciation to design engineers that assisted greatly in this joint effort between Caltrans and the University of Nevada, Reno. Saad El-Azazy from Caltrans was the lead in this cooperative effort. Caltrans is also acknowledged for their financial support. The authors would like to thank Patrick Laplace and Paul Lucas for their work in the Large-Scale Structures Laboratory at the University of Nevada, Reno. The opinion expressed in this paper are those of the authors and do not necessarily represent the opinions of the sponsor.

7.0 REFERENCES

Anthony V. Sanchez, Frieder Seible, and M.J. Nigel Priestley (1997). Seismic Performance of Flared Bridge Columns, *Report No. SSRP-97/0*6, The University of California, San Diego.

Caltrans Seismic Design Criteria, Version 1.1 (July 1999). Caltrans, Sacramento, CA

DIANA User's Manuals, TNO Building and Construction Research Inc., Netherlands, 1999.

Nada, Hisham, David Sanders, M. Saiid Saiidi (2003). Seismic Performance of RC Bridge Frames with Architectural Flared Columns. CCEER#03-01, University of Nevada, Reno, Department of Civil Engineering, pp 476.

Table 1: Summary of model and prototype dimensions.

Description	Prototype	Model	Factor
Column Diameter (mm)	1,524	304.8	0.2
Flare Width (mm)	3,175	635	0.2
Column Reinforcement	30 # 44 mm	14 # 13 mm	1
Column Reinforcement Ratio	2.39	2.4	1
Column Spirals	19 mm @ 101.6	4.88 mm @ 31.75	N/A
Spiral Volume Ratio ($2A_b/SD$)	0.0037	0.0039	1
Column Height (mm)	8,128	1,626	0.2

	LFCD1	LFCD2
Transverse Reinforcement at top 1/3 of the flare	4.88 Dia. @ 27.9 mm	3.76 Dia. @ 96.5 mm
Transverse Ratio	0.439 %	0.075 %
Transverse reinforcement at remaining 2/3 of flare height	3.76 Dia. @ 96.5 mm	3.76 Dia. @ 96.5 mm
Transverse Ratio	0.075 %	0.075 %
Vertical Flare Reinforcement	6 Wires – 3.76 mm Dia.	6 Wires - 3.76 mm Dia.

Table 2: Reinforcement yield stress

Reinforcement Diameter	Yield Point (MPa)
15.9 mm	482
12.7 mm	427
9.5 mm	448
Dia. 4.88 mm	418
Dia. 3.73 mm	491

Table 3: Concrete compressive strength on testing day (MPa)

Member	LFCD1	LFCD2
Footing	35.2	47.4
Columns	37.4	43.6
Girder	38.4	36.2

Table 4: Summary of test observations

Factor	LFCD1 Observations	LFCD2 Observations
0.15 - 0.5	Minor cracking in the beam-column connection and the column.	Minor cracking appears in beam-column connection and in flare region.
0.75 & 1.0	Cracks increased in the beam-column connection and initial cracks in the flare region.	A significant increase of cracking in the beam-column connection occurred. Flare cracks increased in length and new cracks started to form.
1.25	A significant increase of cracking in the beam-column connection occurred	Minor crack development in beam-column connection. Shear and flexural cracks appeared in flare region. Concrete cover spalling in the top of the flare.
1.5 & 1.75	Cracks formation in the beam-column connection drops while the number and extension of diagonal cracks in the flares increases	Crack formation stopped in beam-column connection while flexural and shear cracks increased in the flare and in the bottom of the column.
2.0 & 2.125	Flare cracks increased and widened. Concrete spalling was observed in the middle third of the column and at the top of the flare	Flare cracks increased and widened. Shear cracks along the column height. Extensive concrete spalling occurred in top portion of the flare region.
Last two 1.75	Extensive shear cracking extends along the column height. Displacement was equivalent to 2.125 Sylmar	Flare cracks increased extensively and widened. Concrete spalling in top portion of the flare region. Second 1.75 Sylmar is not included
After bucket removal	Many wide shear cracks were found in the beam and extensive flexural cracks in the middle of the span.	Shear cracks were found in the beam and few flexural cracks in the middle of the span.
Yield Displacement (experimentally calculated)	12.7 mm	12.7 mm
Yield Force	93.4 KN	93.4 KN
Maximum Achieved Displacement	184 mm	184 mm
Maximum Force	282.5 KN	266.9 KN
Ductility Ratio (Includes base slip)	14.5	14.5
Displacement at Gap Closure	69.9 mm	69.9 mm
Ductility at Gap Closure	5.5	5.5

Table 5: Summary of maximum strain

Factor	LFCD2				LFCD2			
	Column		Flare		Column		Flare	
	Long. Steel	Spiral	Long. Steel	Hoops	Long. Steel	Spiral	Long. Steel	Hoops
0.15 & 0.5	0.0029	0.00067	0.0401	0.0145	0.0016	0.002	0.009	0.0037
0.75 & 1	0.013	0.0016	0.0402	0.0145	0.011	0.0028	0.012	0.0053
1.25	0.0144	0.004	0.014	0.017	0.013	0.009	0.014	0.0013
1.5 & 1.75	0.016	0.0037	0.017	0.0145	0.017	0.004	0.013	0.0023
2 & 2.125	0.018	0.002	0.0402	0.0145	0.026	0.007	0.024	0.0033
1.75	0.05	0.0019	0.0403	0.014	N/A	0.0085	0.039	0.0033
1.75	0.05	0.003	0.0403	0.014	N/A	N/A	N/A	N/A

Table 6: Analytical and Experimental results for LFCD1 & LFCD2

	LFCD1	Measured	% of Measured	LFCD2	Measured	% of Measured
Yield force [KN]	228.2	210.3	108%	220.2	203.3	108.3%
Max. Force [KN]	314.4	284.2	N/A	298.0	268.6	N/A
Max. Disp. [mm]	182.9	165.1	N/A	185.2	165.2	N/A
Effective Disp. [mm]	20.8	23.4	89%	24.4	23.9	102%
Displacement Ductility	8.78	7.07	124%	7.59	6.9	110%
Disp. at West Flare Gap Closure [mm]	74.9	67.3	111%	74.7	64.8	115.3%
Disp. at East Flare Gap Closure [mm]	76.2	N/A	N/A	74.7	N/A	N/A
Disp. at West Base Hinge Gap Closure [mm]	109.2	N/A	N/A	110.5	N/A	N/A
Disp. at East Base Hinge Gap Closure [mm]	144.8	N/A	N/A	144.8	N/A	N/A

Table 7: STM results versus experimental results

Specimen	First yield plateau (KN)			Maximum load (KN)		
	Measured	STM	% of Measured	Measured	STM	% of Measured
LFCD1	205.9	197.7	96%	284.2	274.0	96%
LFCD2	203.6	197.7	97%	268.6	274.0	102%

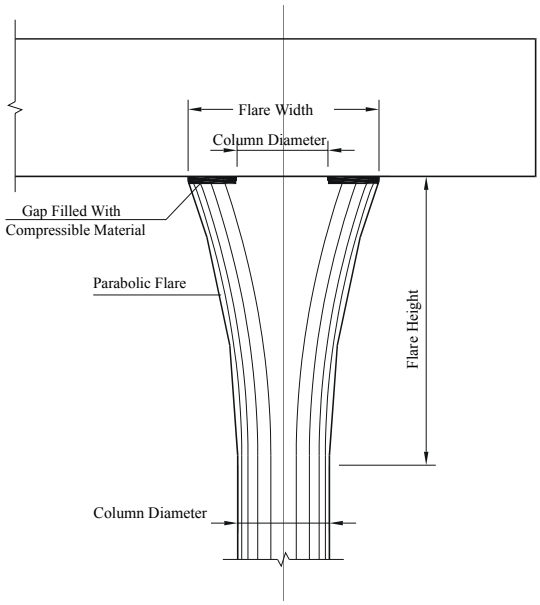

Figure 1: Layout of the proposed detail

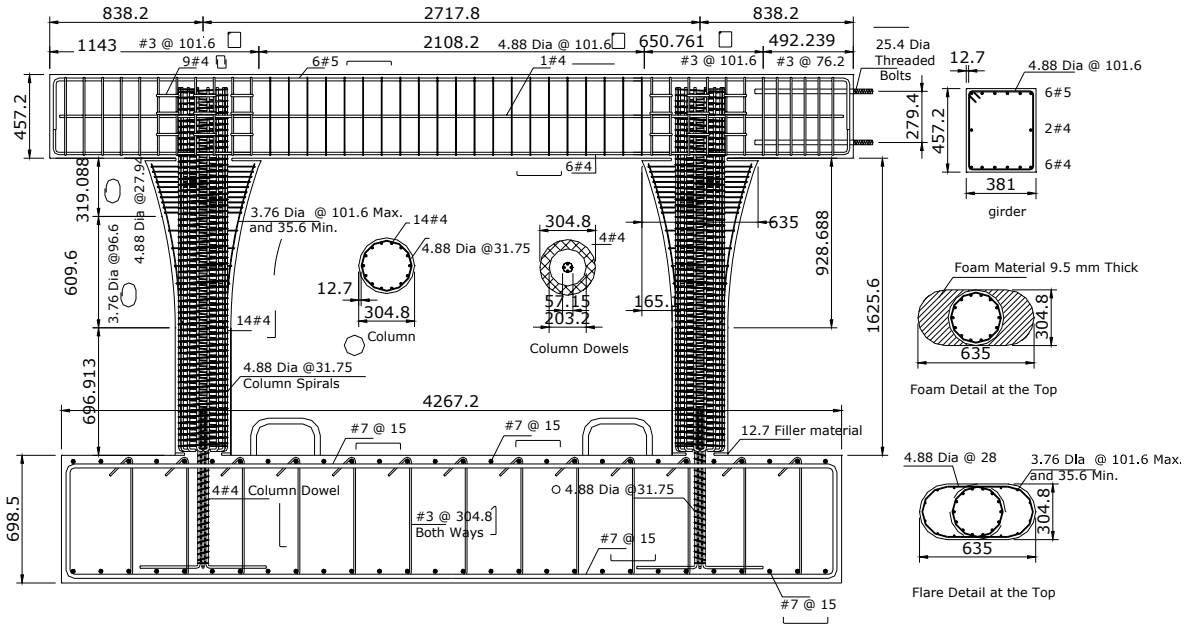

Figure 2: Specimen LFCD1 layout and reinforcement detailing

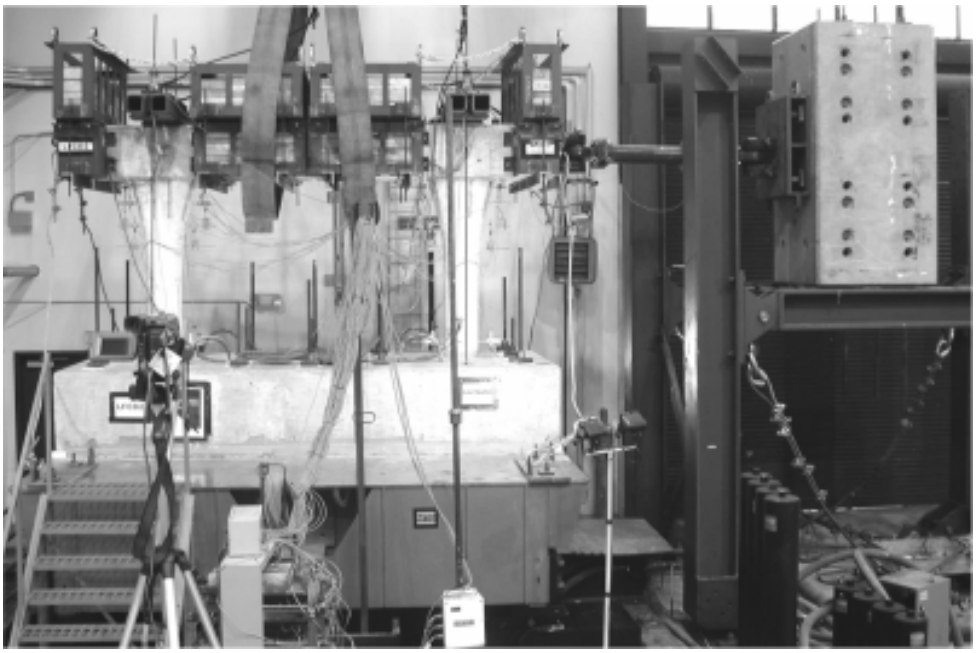

Figure 3: Test setup

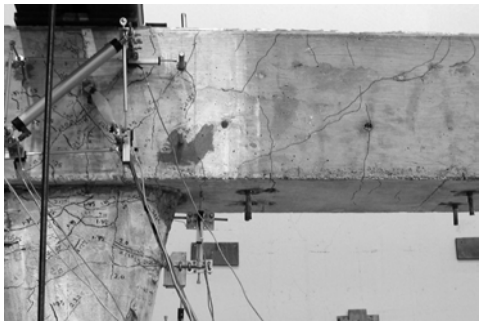

(a)

(b)

(c)

Figure 4: LFCD1 crack patterns, (a) shear cracks in the beam, (b) beam column connection cracks, (c) column cracks

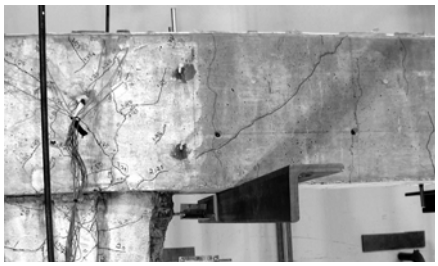

(a)

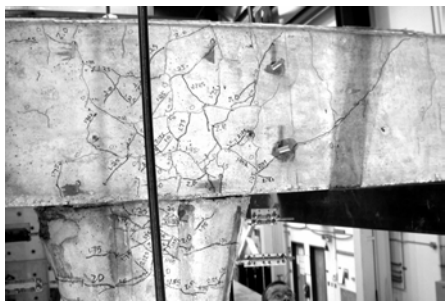

(b)

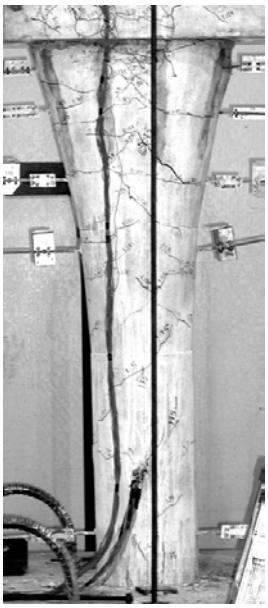

(c)

Figure 5: LFCD2 crack patterns, (a) shear cracks in the beam, (b) beam column connection cracks, (c) column cracks

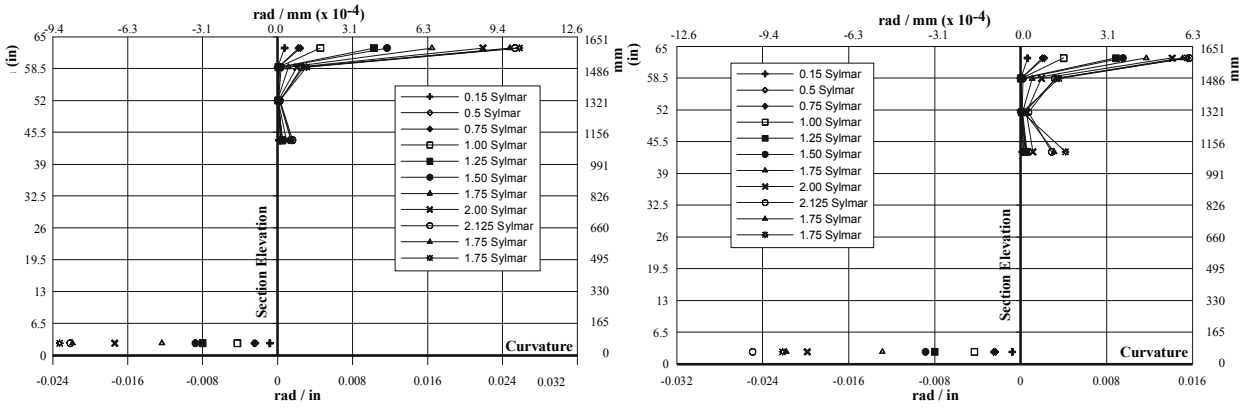

(a) (b)

Figure 6: Curvature along flare height for LFCD1 (a) Left Column (b) Right Column

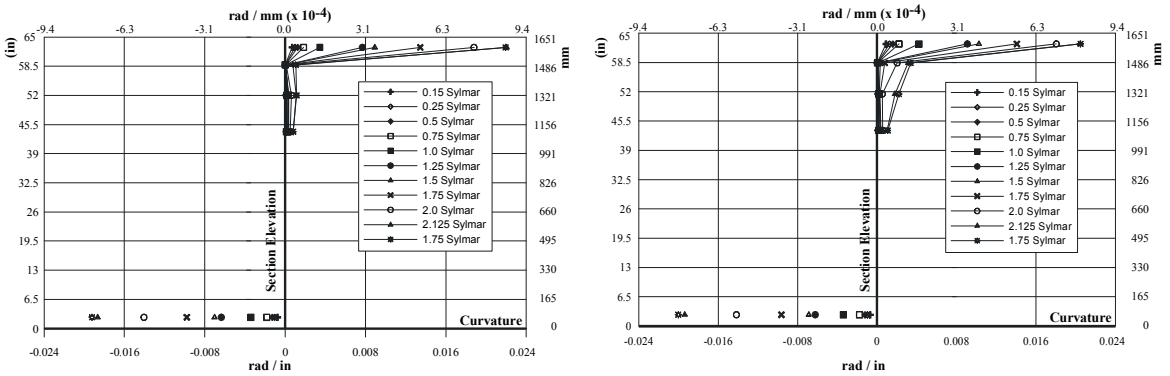

(a) (b)

Figure 7: Curvature along flare height for LFCD2 (a) Left Column (b) Right Column

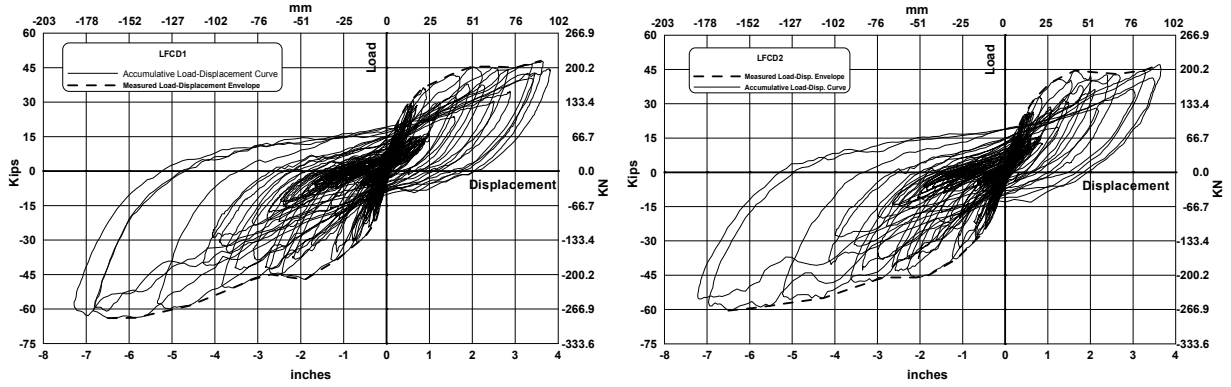

(a) (b)

Figure 8: Accumulative load-displacement curve, (a) LFCD1, (b) LFCD2

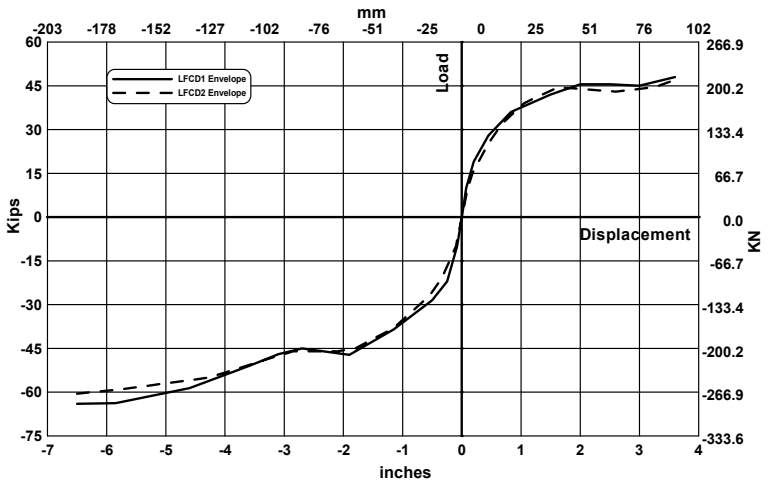

Figure 9: Load-displacement envelope curve

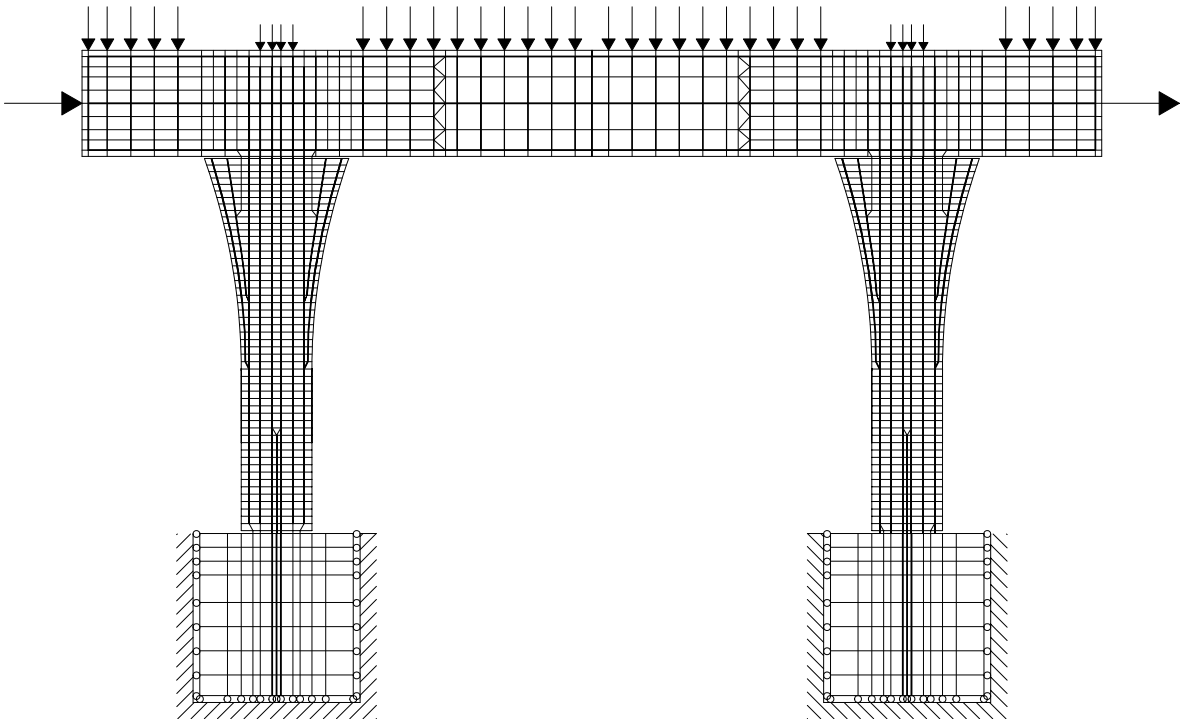

Figure 10: Finite element model

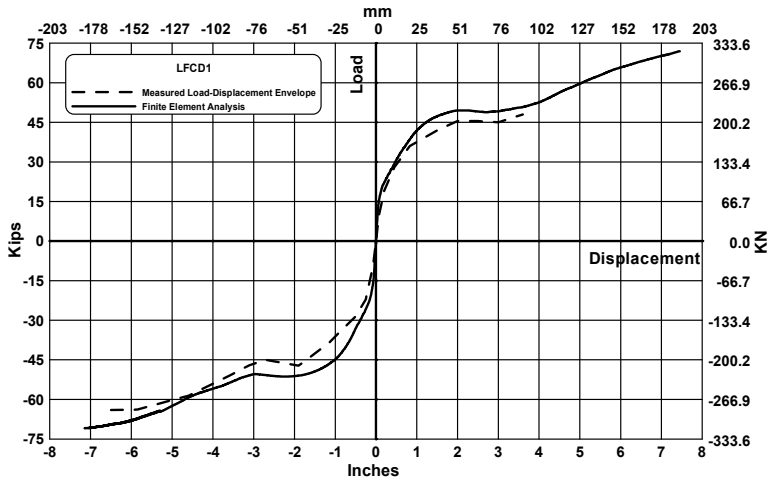

Figure 11: Analytical Results versus Experimental Results for LFCD1

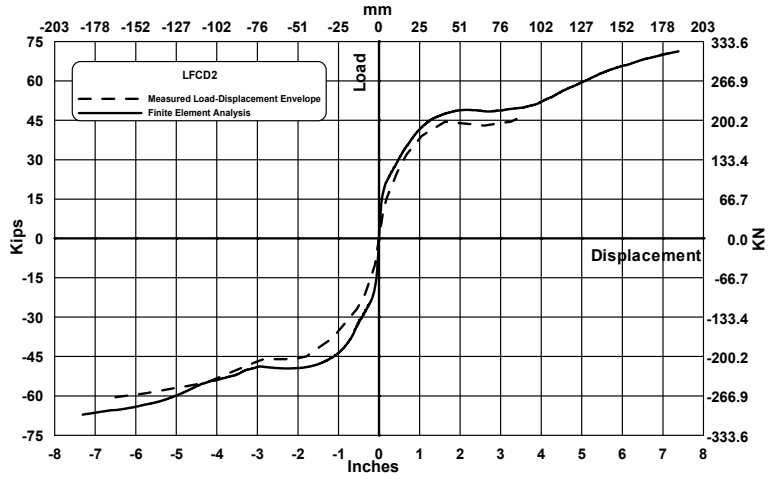

Figure 12: Analytical Results versus Experimental Results for LFCD2

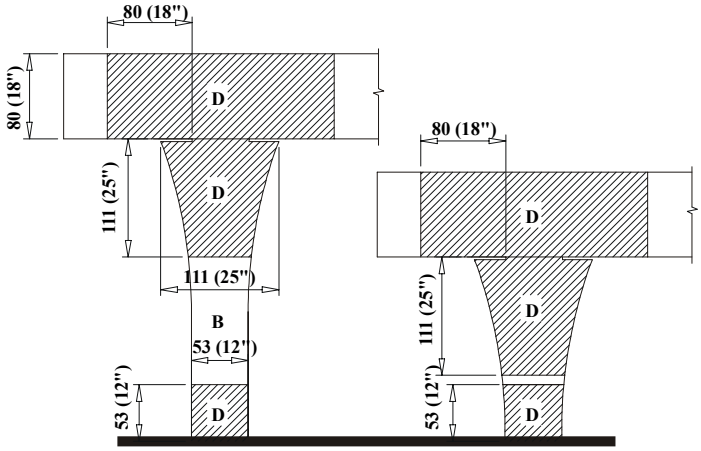

Figure 13: D-Regions and B-Regions for flared columns with a gap

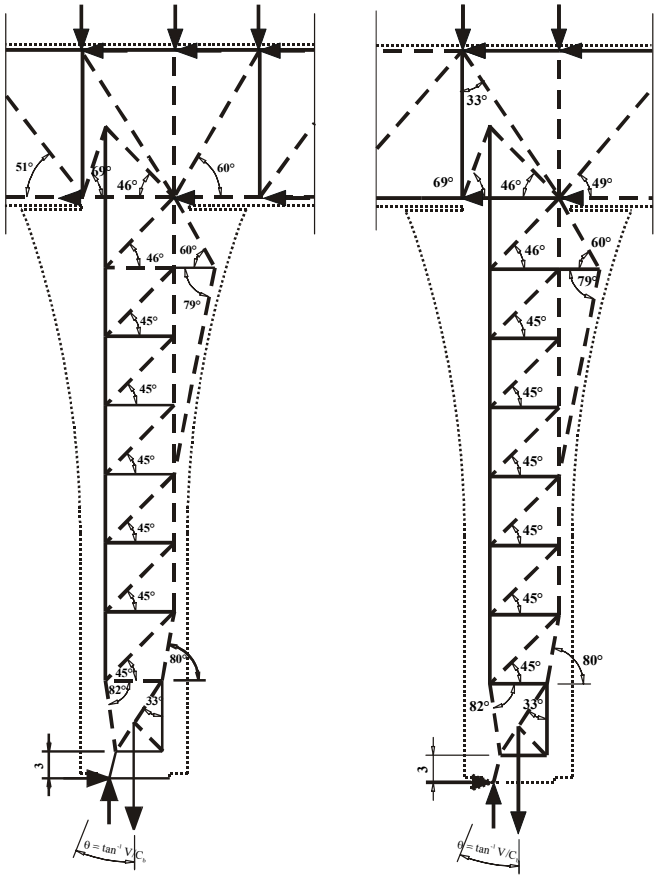

Figure 14: Strut-and-tie model for left and right columns